J|A|C|S
ARTICLES
Published on Web 06/15/2005

Functional Single-Wall Carbon Nanotube Nanohybrids—Associating SWNTs with Water-Soluble Enzyme Model Systems

Dirk M. Guldi,* G. M. Aminur Rahman, Norbert Jux,* Domenico Balbinot, Uwe Hartnagel, Nikos Tagmatarchis, and Maurizio Prato*

Contribution from the Institute for Physical and Theoretical Chemistry, Egerlandstrasse 3, 91058 Erlangen, Germany, Institut für Organische Chemie, Friedrich-Alexander-Universität Erlangen-Nürnberg, Henkestrasse 42, 91054 Erlangen, Germany, and Dipartimento di Scienze Farmaceutiche, Università di Trieste, Piazzale Europa 1, 34127 Trieste, Italy

Received February 14, 2005; E-mail: dirk.guldi@chemie.uni-erlangen.de

Abstract: We succeeded in integrating single-wall carbon nanotubes (**SWNT**s), several water-soluble pyrene derivatives (**pyrene**$^-$), which bear negatively charged ionic headgroups, and a series of water-soluble metalloporphyrins (**MP**$^{8+}$) into functional nanohybrids through a combination of associative van der Waals and electrostatic interactions. The resulting **SWNT/pyrene**$^-$ and **SWNT/pyrene**$^-$**/MP**$^{8+}$ were characterized by spectroscopic and microscopic means and were found to form stable nanohybrid structures in aqueous media. A crucial feature of our **SWNT/pyrene**$^-$ and **SWNT/pyrene**$^-$**/MP**$^{8+}$ is that an efficient exfoliation of the initial bundles brings about isolated nanohybrid structures. When the nanohybrid systems are photoexcited with visible light, a rapid intrahybrid charge separation causes the reduction of the electron-accepting **SWNT** and, simultaneously, the oxidation of the electron-donating **MP**$^{8+}$. Transient absorption measurements confirm that the radical ion pairs are long-lived, with lifetimes in the microsecond range. Particularly beneficial are charge recombination dynamics that are located deep in the Marcus-inverted region. We include, for the first time, work devoted to exploring and testing **FeP**$^{8+}$ and **CoP**$^{8+}$ in donor—acceptor nanohybrids.

Introduction

Nanoscale science, engineering, and technology are emerging fields where scientists and engineers are beginning to manipulate matter at the atomic and molecular scale levels, which leads to dramatically improved materials and device properties.[1]

Carbon nanotubes and, in particular, single-wall carbon nanotubes (**SWNT**), are true examples of nanotechnology.[2−4] **SWNT** are cylindrical carbon molecules (i.e., hollow cores and large aspect ratios) with properties that make them potentially useful in extremely small scale electronic and mechanical applications. They exhibit unusual electronic, mechanical, and adsorptive properties as well as good chemical stability.[5−7] Their unique strength stems from their bonding structure; namely, they are composed entirely of sp^2 bonds, which are appreciably stronger than the sp^3 bonds in diamond.

SWNT have structures similar to those of fullerenes, but while a fullerene molecule is spherical, a nanotube is a one-dimensional nanowire, with one end typically being capped with half a fullerene molecule. In this light, it is possible to envisage that **SWNT** accept electrons readily and transport them with quasi-ballistic features along the tube axis.[8] The high electron

(1) (a) *Introduction to Nanotechnology*; Poole, C. P., Owens, F. J., Eds.; Wiley-Interscience: Weinheim, 2003. (b) *Nanophysics and Nanotechnology: An Introduction to Modern Concepts in Nanoscience*; Wolf, E. L., Ed.; John Wiley & Sons: New York, 2004.
(2) (a) Harris, P. *Carbon Nanotubes and Related Structures: New Materials for the Twenty-First Century*; Cambridge University Press: Cambridge, 2001. (b) *Carbon Nanotubes: Synthesis, Structure, Properties and Applications*; Dresselhaus, M. S., Dresselhaus, G., Avouris, P., Eds.; Springer: Berlin, 2001. (c) Reich, S.; Thomsen, C.; Maultzsch, J. *Carbon Nanotubes: Basic Concepts and Physical Properties*; VCH: Weinheim, 2004.
(3) Special issue on Carbon Nanotubes. *Acc. Chem. Res.* **2002**, *35*, 997.
(4) For recent reviews, see: (a) Hirsch, A. *Angew. Chem., Int. Ed.* **2002**, *41*, 1853. (b) Bahr, J. L.; Tour, J. M. *J. Mater. Chem.* **2002**, *12*, 1952. (c) Niyogi, S.; Hamon, M. A.; Hu, H.; Zhao, B.; Bhomwik, P.; Sen, R.; Itkis, M. E.; Haddon, R. C. *Acc. Chem. Res.* **2002**, *35*, 1105. (d) Sun, Y.-P.; Fu, K.; Lin, Y.; Huang, W. *Acc. Chem. Res.* **2002**, *35*, 1096. (e) Banerjee, S.; Kahn, M. G. C.; Wang, S. S. *Chem. Eur. J.* **2003**, *9*, 1898. (f) Tasis, D.; Tagmatarchis, N.; Georgakilas, V.; Prato, M. *Chem. Eur. J.* **2003**, *9*, 4000. (g) Dyke, C. A.; Tour, J. M. *Chem. Eur. J.* **2004**, *10*. 812.
(5) (a) Kong, J.; Franklin, N. R.; Zhou, C. W.; Chapline, M. G.; Peng, S.; Cho, K. J.; Dai, H. J. *Science* **2000**, *287*, 622. (b) Goldoni, A.; Larciprete, R.; Petaccia, L.; Lizzit, S. *J. Am. Chem. Soc.* **2003**, *125*, 11329.
(6) (a) Baughman, R. H.; Cui, C. X.; Zakhidov, A. A.; Iqbal, Z.; Barisci, J. N.; Spinks, G. M.; Wallace, G. G.; Mazzoldi, A.; De Rossi, D.; Rinzler, A. G.; Jaschinski, O.; Roth, S.; Kertesz, M. *Science* **1999**, *284*, 1340. (b) Mamedov, A. A.; Kotov, N. A.; Prato, M.; Guldi, D. M.; Wicksted, J. P.; Hirsch, A. *Nature Mater.* **2002**, *1*, 190. (c) Dalton, A. B.; Collins, S.; Munoz, E.; Razal, J. M.; Ebron, V. H.; Ferraris, J. P.; Coleman, J. N.; Kim, B. G.; Baughman, R. H. *Nature* **2003**, *423*, 703.
(7) (a) Sorescu, D. C.; Jordan, K. D.; Avouris, P. *J. Phys. Chem. B* **2001**, *105*, 11227. (b) Javey, A.; Guo, J.; Wang, Q.; Lundstrom, M.; Dai, H. J. *Nature* **2003**, *424*, 654.
(8) (a) Georgakilas, V.; Kordatos, K.; Prato, M.; Guldi, D. M.; Holzinger, M.; Hirsch, A. *J. Am. Chem. Soc.* **2002**, *124*, 760. (b) Murakami, H.; Nomura, T.; Nakashima, N. *Chem. Phys. Lett.* **2003**, *378*, 481. (c) Guldi, D. M.; Marcaccio, M.; Paolucci, D.; Paolucci, F.; Tagmatarchis, N.; Tasis, D.; Vazquez, E.; Prato, M. *Angew. Chem., Int. Ed.* **2003**, *42*, 4206. (d) Li, H.; Zhou, B.; Gu, L.; Wang, W.; Shiral Ferando, K. A.; Kumar, S.; Allard, J. F.; Sun, Y.-P. *J. Am. Chem. Soc.* **2004**, *126*, 1014. (e) Guldi, D. M.; Rahman, G. M. A.; Ramey, J.; Marcaccio, M.; Paolucci, D.; Paolucci, F.; Qin, S.; Ford, W. T.; Balbinot, D.; Jux, N.; Tagmatarchis, N.; Prato, M. *Chem. Commun.* **2004**, 2034.

 10.1021/ja050930o CCC: $30.25

mobility — with values that are 25% higher than in any other known semiconductor material — further strengthens this assumption.[9] Thus, **SWNT**s may find a prominent place in electro- and photoactive nanocomposites with high surface areas — just as other carbon modifications/allotropes have been tested successfully as electron acceptors in recent research.[10] However, before **SWNT** may be integrated into functional arrays (i.e., donor−acceptor nanohybrids) or tested in practical applications (i.e., photovoltaic devices), several key issues need to be properly addressed. One of them entails the control over modifying the **SWNT** surface with functional groups, such as chromophores,[11] electron donors,[12] biomolecules, etc.[13]

High degrees of functionalization alter appreciably the π-electronic structure and, subsequently, the properties of **SWNT**.[14] On one hand, the shape and size of functionalized **SWNT** are largely retained. On the other hand, each cycloaddition step eliminates an equal number of π-electrons from the curved surface,[15] though the electronic structure of the carbon framework is governed by the graphenic π-electrons.[16] Thus, **SWNT** functionalization corresponds to doping, which affects (i) the band gaps and (ii) the long-range conjugation.[17] With an eye on keeping the electronic properties of **SWNT** intact, alternative strategies are needed to develop donor−acceptor **SWNT** nanohybrids. In particular, concepts should be considered that assist in controlling contacts between electron donors and electron acceptors while preserving the π-electronic structure of **SWNT**. Supramolecular concepts fulfill such requisites. Additional incentives that call for supramolecular means (i.e., polymer wrapping, $\pi-\pi$ interactions, etc.) are their flexibility and tunability.[18,19]

We have shown earlier that cationic and anionic porphyrins form ensembles with charged fullerene and **SWNT** derivatives.[10e,19b,20] Interestingly, electrostatic forces play crucial roles in maintaining the tertiary and quarternary structure of enzymes and also in their interactions with other biomolecules.[21] An excellent example is the hybridization of cytochrome *c* with cytochrome *c* oxidase. As the terminal enzyme in the respiratory chain, cytochrome *c* oxidase catalyzes the reduction of dioxygen to water and pumps an additional proton across the membrane for each proton consumed in the reaction.[22] Although supramolecular complexes of charged metalloporphyrins and **SWNT** are certainly no models for heme-containing enzymes, it is reasonable to assume that chemical processes happening in such proteins can be performed in electrostatic **SWNT**/metalloporphyrin aggregates. The electron-accepting and/or charging properties of **SWNT** hint at the possibility of an oxidation catalysis of these aggregates, with the metalloporphyrin acting as the reaction center and the SWNT ensuring the necessary

(9) Dürkop, T.; Getty, S. A.; Cobas, E.; Fuhrer, M. S. *Nano Lett.* **2004**, *4*, 35.

(10) (a) Imahori, H.; Sakata, Y. *Adv. Mater.* **1997**, *9*, 537. (b) Prato, M. *J. Mater. Chem.* **1997**, *7*, 1097. (c) Martín, N.; Sánchez, L.; Illescas, B.; Pérez, I. *Chem. Rev.* **1998**, *98*, 2527. (d) Diederich, F.; Gomez-Lopez, M. *Chem. Soc. Rev.* **1999**, *28*, 263. (e) Imahori, H.; Sakata, Y. *Eur. J. Org. Chem.* **1999**, 2445. (f) Guldi, D. M. *Chem. Commun.* **2000**, 321. (g) Guldi, D. M.; Prato, M. *Acc. Chem. Res.* **2000**, *33*, 695. (h) Gust, D.; Moore, T. A.; Moore, A. L. *Acc. Chem. Res.* **2001**, *34*, 40. (i) Guldi, D. M. *Chem. Soc. Rev.* **2002**, *31*, 22. (j) Guldi, D. M.; Prato, M. *Chem. Commun.* **2004**, 2517. (k) Segura, J. L.; Martín, N.; Guldi, D. M. *Chem. Soc. Rev.* **2005**, *34*, 31.

(11) (a) Qu, L. W.; Martin, R. B.; Huang, W. J.; Fu, K. F.; Zweifel, D.; Lin, Y.; Sun, Y. P.; Bunker, C. E.; Harruff, B. A.; Gord, J. R.; Allard, L. F. *J. Chem. Phys.* **2002**, *117*, 8089. (b) Georgakilas, V.; Kordatos, K.; Prato, M.; Guldi, D. M.; Holzinger, M.; Hirsch, A. *J. Am. Chem. Soc.* **2002**, *124*, 760. (c) Murakami, H.; Nomura, T.; Nakashima, N. *Chem. Phys. Lett.* **2003**, *378*, 481. (d) Li, H.; Zhou, B.; Lin, Y.; Gu, L.; Wang, W.; Fernando, K. A. S.; Kumar, S.; Allard, L. F.; Sun, Y.-P. *J. Am. Chem. Soc.* **2004**, *126*, 1014. (e) Alvaro, M.; Atienzar, P.; de la Cruz, P.; Delgado, J. L.; Garcia, H.; Langa, F. *J. Phys. Chem. B* **2004**, *108*, 12691. (f) Martin, R. B.; Qu, L. W.; Lin, Y.; Harruff, B. A.; Bunker, C. E.; Gord, J. R.; Allard, L. F.; Sun, Y. P. *J. Phys. Chem. B* **2004**, *108*, 11447. (g) Alvaro, M.; Atienzar, P.; Bourdelande, J. L.; Garcia, H. *Chem. Phys. Lett.* **2004**, *384*, 119.

(12) (a) Kymakis, E.; Amaratunga, G. A. J. *Appl. Phys. Lett.* **2002**, *80*, 112. (b) Kymakis, E.; Amaratunga, G. A. J. *Sol. Energy Mater. Sol. Cells* **2003**, *80*, 465. (c) Kymakis, E.; Alexandrou, I. *J. Appl. Phys.* **2003**, *93*, 1764. (d) Yang, C.; Wohlgenannt, M.; Vardeny, Z. V.; Blau, W. J.; Dalton, A. B.; Baughman, R.; Zakhidov, A. A. *Physica B* **2003**, *338*, 366. (e) Sheeney-Hai-Ichia, L.; Basnar, B.; Willner, I. *Angew. Chem., Int. Ed.* **2005**, *44*, 78.

(13) (a) Chen, R. J.; Zhang, Y.; Wang, D.; Dai, H. *J. Am. Chem. Soc.* **2001**, *123*, 3838. (b) Shim, M.; Kim, N. W. S.; Chen, R. J.; Li, Y.; Dai, H. *Nano Lett.* **2002**, *2*, 285. (c) Pantarotto, D.; Partidos, C. D.; Graff, R.; Hoebeke, J.; Briand, J.-P.; Prato, M.; Bianco, A. *J. Am. Chem. Soc.* **2003**, *125*, 6160. (d) Chou, S. G.; Ribeiro, H. B.; Barros, E. B.; Santos, A. P.; Nezich, D.; Samsonidze, G. G.; Fantini, C.; Pimenta, M. A.; Jorio, A.; Plentz, F.; Dresselhaus, M. S.; Dresselhaus, G.; Saito, R.; Zheng, M.; Onoa, G. B.; Semke, E. D.; Swan, A. K.; Unlu, M. S.; Goldberg, B. B. *Chem. Phys. Lett.* **2004**, *397*, 296. (e) Yeh, I. C.; Hummer, G. *Proc. Natl. Acad. Sci.* **2004**, *101*, 12177. (f) Lin, Y.; Taylor, S.; Li, H. P.; Fernando, K. A. S.; Qu, L. W.; Wang, W.; Gu, L. R.; Zhou, B.; Sun, Y. P. *J. Mater. Chem.* **2004**, *14*, 527. (g) Zheng, M.; Jagota, A.; Strano, M. S.; Santos, A. P.; Barone, P.; Chou, S. G.; Diner, B. A.; Dresselhaus, M. S.; McLean, R. S.; Onoa, G. B.; Samsonidze, G. G.; Semke, E. D.; Usrey, M.; Walls, D. J. *Science* **2004**, *302*, 1545.

(14) (a) Dillon, A. C.; Gennett, T.; Jones, K. M.; Alleman, J. L.; Parilla, P. A.; Heben, M. J. *Adv. Mater.* **1999**, *11*, 1354. (b) Chiang, W.; Brinson, B. E.; Smalley, R. E.; Margrave, J. L.; Hauge, R. H. *J. Phys. Chem. B* **2001**, *105*, 1157. (c) Strano, M. S.; Dyke, C. A.; Usrey, M. L.; Barone, P. W.; Allen, M. J.; Shan, H.; Kittrell, C.; Hauge, R. H.; Tour, J. M.; Smalley, R. E. *Science* **2003**, *301*, 1519. (d) Zurek, E.; Autschbach, J. *J. Am. Chem.* Soc. **2004**, *120*, 13079.

(15) (a) Georgakilas, V.; Voulgaris, D.; Vazquez, E.; Prato, M.; Guldi, D. M.; Kukovecz, A.; Kuzmany, H. *J. Am. Chem. Soc.* **2002**, *124*, 14318. (b) Guldi, D. M.; Holzinger, M.; Hirsch, A.; Georgakilas, V.; Prato, M. *Chem. Commun.* **2003**, 1130.

(16) (a) Chico, L.; Crespi, V. H.; Benedict, L. X.; Louie, S. G.; Cohen, M. L. *Phys. Rev. Lett.* **1996**, *76*, 971. (b) Carroll, D. L.; Redlich, P.; Ajayan, P. M.; Charlier, J. C.; Blasé, X.; DeVita, A.; Car, R. *Phys. Rev. Lett.* **1997**, *78*, 2811. (c) Maarouf, A. A.; Kane, C. L.; Mele, E. J. *Phys. Rev.* **2000**, *61*, 11156. (d) Lemay, S. G.; Janssen, J. W.; van den Hout, M.; Mooij, M.; Bronikowski, M. J.; Willis, P. A.; Smalley, R. E.; Kouwenhoven, L. P.; Dekker: C. *Nature* **2001**, *412*, 617. (e) Avouris, P. *Chem. Phys.* **2002**, *281*, 429. (f) Brandbyge, M.; Mozos, J. L.; Ordejon, P.; Taylor, J.; Stokbro, K. *Phys. Rev. B* **2002**, *65*, 165401.

(17) Melle-Franco, M.; Marcaccio, M.; Paolucci, D.; Paolucci, F.; Georgakilas, V.; Guldi, D. M.; Prato, M.; Zerbetto, F. *J. Am. Chem. Soc.* **2004**, *126*, 1646.

(18) (a) Hamon, M. A.; Chen, J.; Hu, H.; Chen, Y.; Itkis, M. E.; Rao, A. M.; Eklund, R. C.; Haddon, R. C. *Adv. Mater.* **1999**, *11*, 834. (b) Tang, B. Z.; Xu, H. *Macromolecules* **1999**, *32*, 2569. (c) Coleman, J. N.; Dalton, A. B.; Curran, S.; Rubio, A.; Davey, A. P.; Drury, A.; McCarthy, B.; Lahr, B.; Ajayan, P. M.; Roth, S.; Barklie, R. C.; Blau, W. J. *Adv. Mater.* **2000**, *12*, 213. (d) Dalton, A. B.; Stephan, C.; Coleman, J. N.; McCarthy, B.; Ajayan, P. M.; Lefrant, S.; Bernier, P.; Blau, W. J. *J. Phys. Chem.* **2000**, *104*, 10012. (e) Star, A.; Stoddart, J. F.; Steuerman, D.; Dile, M.; Boukai, A.; Wong, E. W.; Yang, X.; Cheng, S. W.; Choi, H.; Heath, J. R. *Angew. Chem., Int. Ed.* **2001**, *40*, 1721. (f) Chen, J.; Liu, H. Y.; Weimer, W. A.; Halls, M. D.; Waldeck, D. H.; Walker, G. C. *J. Am.* Chem. Soc. **2002**, *124*, 9034. (g) Star, A.; Steuerman, D. W.; Heath, J. R.; Stoddart, J. F. *Angew. Chem., Int. Ed.* **2002**, *41*, 2508. (h) Star, A.; Liu, Y.; Grant, K.; Ridvan, L.; Stoddart, J. F.; Steuerman, D. W.; Diehl, M. R.; Boukai, A.; Heath, J. R. *Macromolecules* **2003**, *36*, 553. (i) Numata, M.; Asai, M.; Kaneko, K.; Hasegawa, T.; Fujita, N.; Kitada, Y.; Sakurai, K.; Shinkai, S. *Chem. Lett.* **2004**, *33*, 232. (j) Guldi, D. M.; Taieb, H.; Rahman, G. M. A.; Tagmatarchis, N.; Prato, M. *Adv. Mater.* **2005**, *17*, 871.

(19) (a) Nakashima, N.; Tomonari, Y.; Murakami, H. *Chem. Lett.* **2002**, 638. (b) Guldi, D. M.; Rahman, G. M. A.; Tagmatarchis, N.; Prato, M. *Angew. Chem., Int. Ed.* **2004**, *43*, 5526. (c) Artyukhin, A. B.; Bakajin, O.; Stroeve, P.; Noy, A. *Langmuir* **2004**, *20*, 1442. (d) Fifield, L. S.; Dalton, L. R.; Addleman, R. S.; Galhotra, R. A.; Engelhard, M. H.; Fryxell, G. E.; Aardahl, C. L. *J. Phys. Chem. B* **2004,** *108*, 8737. (e) Zhu, J.; Yudasaka, M.; Zhang, M. F.; Iijima, S. *J. Phys. Chem. B* **2004**, *108*, 11317.

(20) Balbinot, D.; Atalick, S.; Guldi, D. M.; Hatzimarinaki, M.; Hirsch, A.; Jux, N. *J. Phys. Chem. B* **2003**, *107*, 13273.

(21) (a) Isied, S. S.; Worosila, G.; Artherton, S. J. *J. Am. Chem. Soc.* **1982**, *104*, 7659. (b) Isied, S. S. *ACS Adv. Chem. Ser.* **1997**, *253*, 331. (c) McArdle, J. V.; Gray, H. B.; Creutz, C.; Sutin, N. *J. Am. Chem. Soc.* **1974**, *96*, 5737. (d) McArdle, J. V.; Yocon, K.; Gray, H. B. *J. Am. Chem. Soc.* **1977**, *12*, 4141. (e) Meier, M.; Van Eldik, R. *Inorg. Chim. Acta* **1994**, *225*, 95. (f) Meier, M.; Van Eldik, R.; Chang, I. J.; Mines, G. A.; Wuttke, D. S.; Winkler, J. R.; Gray, H. B. *J. Am. Chem. Soc.* **1994**, *116*, 1577. (g) Meier, M.; Sun, J.; Ban Eldik, R.; Wishart, J. F. *Inorg. Chem.* **1996**, *35*, 1564. (h) Meier, M.; Van Eldik, R. *Inorg. Chim. Acta* **1996**, *242*, 185. (i) Meier, M.; Van Eldik, R. *Chem. Eur. J.* **1997**, *3*, 39. (j) Jain, R. K.; Hamilton, A. D. *Angew. Chem., Int. Ed.* **2002**, *41*, 641. (k) Decher, G. *Science* **1997**, *277*, 1232. (l) Kaschak, D. M.; Lean, J.-T.; Waraksa, C. C.; Saupe, G. B.; Usami, H.; Mallouk, T. E. *J. Am. Chem. Soc.* **1999**, *121*, 3435.

(22) (a) FergusonMiller, S.; Babcock, G. T. *Chem. Rev.* **1996**, *96*, 2889. (b) Ostermeier, C.; Iwata, S.; Michel, H. *Curr. Opin. Struct. Biol.* **1996**, *6*, 460. (c) Hill, B. C. *J. Biol. Chem.* **1994**, *269*, 2419.

electron transport.[8,16] In the current work, we introduce a set of new cationic metalloporphyrins, **FeP**$^{8+}$ and **CoP**$^{8+}$, and their systematic integration into novel **SWNT** ensembles.

Crucial for our binding assays — in which two reference systems (i.e., $\mathbf{H_2P}^{8+}$ and $\mathbf{ZnP}^{8+}$) and two novel model systems (i.e., **FeP**$^{8+}$ and **CoP**$^{8+}$) were tested — are **SWNT** templates that bear carboxylate or sulfonate functionalities. These negatively charged groups function as promoters for suspending **SWNT** samples in aqueous media and likewise as anchors to interact with one or several pyridinium headgroups present in the different metalloporphyrins.[19]

Results and Discussion

FeP^{8+} and CoP^{8+}. The syntheses of **FeP**$^{8+}$ and **CoP**$^{8+}$ were accomplished via metalating the octabromomethylated porphyrin $\mathbf{H_2Br_8}$ under standard conditions. $\mathbf{FeBr_8}$ and $\mathbf{CoBr_8}$ were both obtained in moderate to good yields. For $\mathbf{CoBr_8}$, both ^{1}H NMR and UV/vis spectra suggest a paramagnetic low-spin character (i.e., cobalt(II) porphyrin). On the other hand, $\mathbf{FeBr_8}$ is a high-spin iron(III) complex. The axial ligands of $\mathbf{FeBr_8}$ were, in accordance with ^{1}H NMR and microanalysis data, assigned as hydroxide ligands — most likely stemming from a bromide/hydroxide exchange that takes place during the column chromatography.

Next, $\mathbf{FeBr_8}$ and $\mathbf{CoBr_8}$ were reacted with 4-*tert*-butylpyridine to give the desired cationic compounds **FeP**$^{8+}$ and **CoP**$^{8+}$ in 71% and 65% yields, respectively. The ^{1}H NMR spectrum confirms that **FeP**$^{8+}$ remains as a high-spin iron(III) complex with a partially intermediate spin. The high symmetry of the ^{1}H NMR spectrum indicates that the iron cation carries two identical axial ligands, whereas the pyrrole proton resonance at 63.9 ppm indicates an intermediate spin ($S = {}^3/_2$) at the iron center. Both results indicate that two water molecules are bound to the central metal. Surprisingly, the ^{1}H NMR spectra specify that **CoP**$^{8+}$ transformed to a diamagnetic species, although the resonances are somewhat broadened. In the UV/vis spectrum, significant shifts of the Soret and Q-band absorptions of **CoP**$^{8+}$ — compared with those of $\mathbf{CoBr_8}$ — further support the notion that a change in redox state took place. Which axial ligands are bound to the cobalt center, bromide or 4-*tert*-butylpyridine, both present in the reaction mixture, remains, however, an open question. Since (i) no signals appear for the α- and β-pyridine proton resonances and (ii) the total number of signals in the ^{1}H NMR spectrum shows that **CoP**$^{8+}$ still possesses D_{4h} symmetry on the NMR time scale, it is likely that a fast exchange of ligands takes place.[23]

SWNT/Pyrene$^-$. Our approach to form dispersable **SWNT** ensembles involves the immobilization of water-soluble **pyrene**$^-$ derivatives (i.e., 1-pyreneacetic acid (**1**), 1-pyrenecarboxylic acid (**2**), 1-pyrenebutyric acid (**3**), and 8-hydroxy-1,3,6-pyrenetrisulfonic acid (**4**)) with pristine **SWNT** (see Scheme 1). In particular, strong van der Waals forces are operative between the two π-systems. Stable dispersions of **SWNT/pyrene**$^-$ were prepared by stirring, sonicating, and centrifuging 10 mL of a sodium tetraborate decahydrate buffer (pH = 9.2) **pyrene**$^-$ solution (1 mM) with 1 mg of purified **SWNT**. To minimize the amount of free **pyrene**$^-$, which is expected to interfere in the association assays, we isolated the **SWNT/pyrene**$^-$ from the centrifuged solid. This approach bears the advantage to eliminate free **pyrene**$^-$ that is not immobilized onto the **SWNT** surface and leaves mostly the target compounds, **SWNT/pyrene**$^-$.

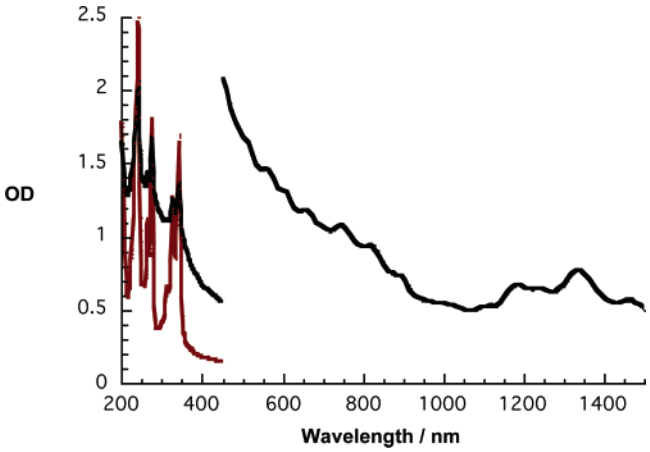

Figure 1. Absorption spectra of dilute solutions of **3** and **SWNT/3**, displaying the UV, visible, and NIR regions. While for the 200−450 nm range H_2O solutions were prepared, the 450−1500 nm range was monitored from a D_2O solution.

The absorption spectra of the typically black **SWNT/pyrene**$^-$ solutions not only feature characteristics of both building blocks but also testify to their mutual interaction. Figure 1 demonstrates this. Here, a typical spectrum of **3** is compared with that of the corresponding **SWNT/3** dispersion, after matching the absorption at 350 nm. Several key features are discernible. First, the 450−1500 nm region reveals the **SWNT** van Hove singularities, which fall into groups of metallic transitions (i.e., E_{11}) in the 500−600 nm range and of semiconductor transitions in the 600−900 nm (i.e., E_{22} semiconductor transitions)/1000−1500 nm regions (i.e., E_{11} semiconductor transitions).[24] Second, the characteristic pyrene transitions in **3** are seen in the 200−400 nm region. Third, insight into van der Waals interactions between **SWNT** and **3** came from bathochromic shifts (i.e., ~2 nm) in **SWNT/3**, which suggests mutually interacting π-systems. Similar data are gathered for the analogous **SWNT** association with **1**, **2**, and **4**. Figure S1 (Supporting Information) reviews the NIR sections of all the different **SWNT/pyrene**$^-$ (i.e., **1**, **2**, **3**, and **4**).

A fundamental advantage for our work is that the pyrene compounds are also strong fluorophores.[25] This feature renders them convenient and sensitive markers for intrahybrid interactions, which when compared in different samples provides valuable insight into excited-state deactivations with **SWNT**. It is important that we and others have recently demonstrated that in covalently linked **SWNT/pyrene** nanohybrids intramolecular fluorescence quenching prevails.[11] The quenching is attributed to intramolecular transduction of singlet excited energy — from the high-energy pyrene singlet excited state to

(23) The open question regarding the axial ligands is of only minor concern, since aqueous buffer solutions are used in the association and electron-transfer studies. Hereby, water or hydroxide ligands will replace any other donor molecule complexed by the central metal. Detailed investigations on the behavior of **FeP**$^{8+}$ and **CoP**$^{8+}$ in aqueous solutions are currently being performed.

(24) (a) O'Connell, M. J.; Bachilo, S. M.; Huffman, C. B.; Moore, V. C.; Strano, M. S.; Haroz, E. H.; Rialon, K. L.; Boul, P. J.; Noon, W. H.; Kittrell, C.; Ma, J. P.; Hauge, R. H.; Weisman, R. B.; Smalley, R. E. *Science* **2002**, *297*, 593. (b) Bachilo, S. M.; Strano, M. S.; Kittrell, C.; Hauge, R. H.; Smalley R. E.; Weisman, R. B. *Science* **2002**, *298*, 2361.

(25) Murov, S. L.; Carmichael, I.; Hug, G. L. *Handbook of Photochemistry*; Dekker: New York, 1993.

Scheme 1. Structures of Compounds Used in This Work

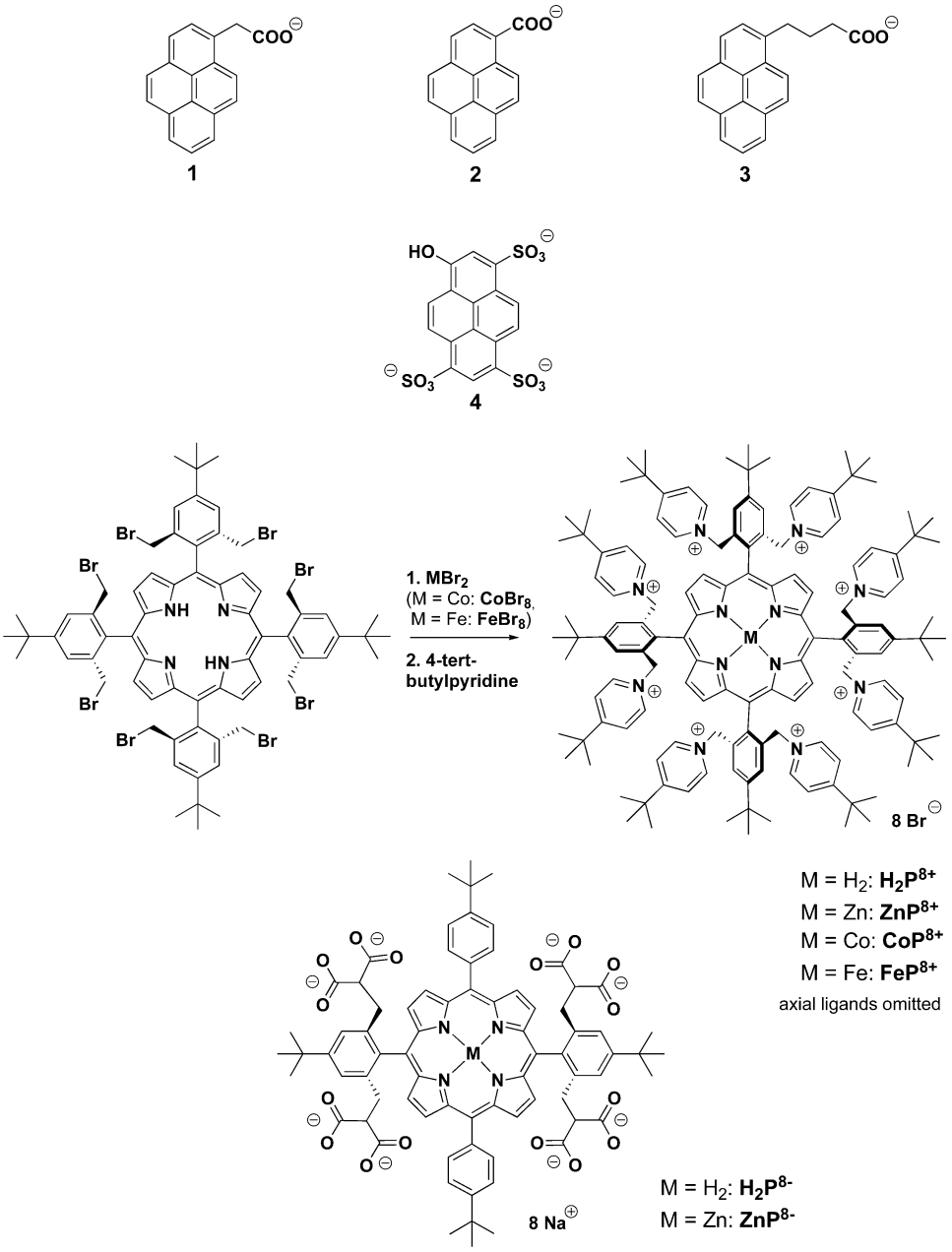

the low-energy manifold of **SWNT**. In line with this conclusion, we see strong fluorescence quenching in all the new **SWNT/pyrene**$^-$ ensembles. The quenching is as strong as 80%, for example, in **SWNT/3**, as shown in Figure 2. A reasonable assumption for the residual fluorescence is free, not immobilized **pyrene**$^-$ in solution.

In parallel with the steady-state experiments, we tested sets of **pyrene**$^-$ and **SWNT/pyrene**$^-$ in time-resolved fluorescence decay measurements. We noted in all four different sets only the long-lived pyrene fluorescence. For example, following the 375 nm fluorescence in oxygen-free samples of **3** and **SWNT/3** led to lifetimes of 93 $\pm$ 2 ns. This confirms our earlier hypothesis that the residual fluorescence, noted in the steady-state experiments, is largely due to non-immobilized **pyrene**$^-$. As far as **SWNT/pyrene**$^-$ interactions are concerned, we have to assume that they happen in a time domain that is essentially covered by our instrumental resolution of around 100 ps. Thus, we can only estimate a lower limit for the intrahybrid deactivation of photoexcited **pyrene**$^-$, $k \gg 2.0 \times 10^{10}$ s^{-1}. However, based on the $\pi-\pi$ stacking in **SWNT/pyrene**$^-$, we have to

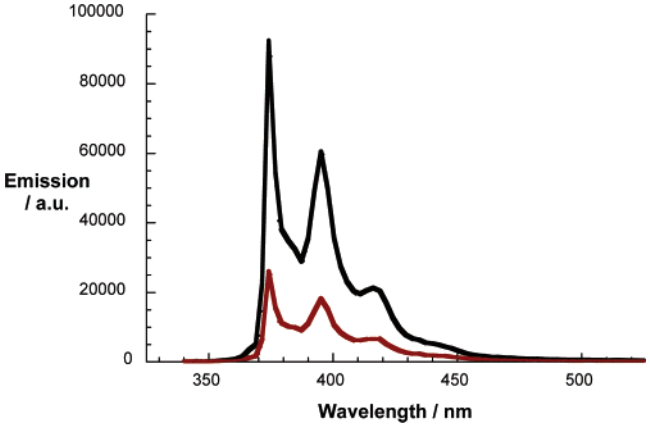

Figure 2. Fluorescence spectra of dilute solutions of **3** and **SWNT/3** that display equal absorption at the 335 nm excitation wavelength.

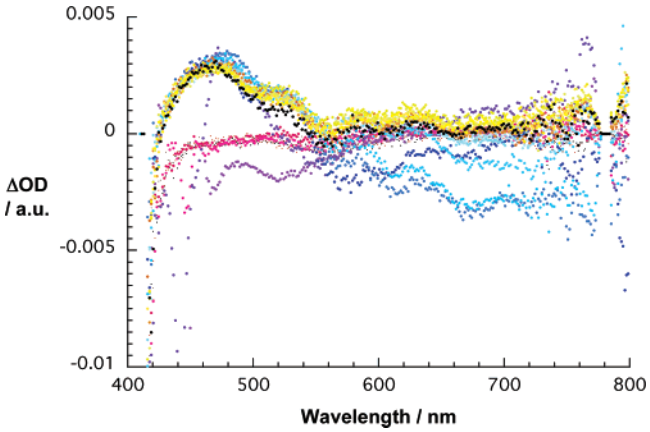

Figure 3. Differential absorption spectrum (visible) obtained upon femtosecond flash photolysis (387 nm) of **SWNT/pyrene**$^-$ in nitrogen-saturated aqueous solutions with several time delays between 0 and 4 ps at room temperature.

consider rates somewhere in the neighborhood of 10^{11} s^{-1}. These values were independently confirmed in femtosecond resolved transient absorption spectroscopic measurements (vide supra).

Exact information on the dynamic excited-state interactions in **SWNT/pyrene**$^-$ was obtained by utilizing transient absorption changes starting with a fast 150 fs excitation at 387 nm. For **pyrene**$^-$ alone, characteristic long-lived singlet−singlet features develop (no significant decay on the 1500 ps time scale). An ultrafast deactivation, on the other hand, is seen for the same **pyrene**$^-$-centered features in **SWNT/pyrene**$^-$ as summarized in Figure 3 for **3**. From the corresponding time−absorption profiles (see Figure S2, Supporting Information), a rate constant of $(1.8 \pm 0.3) \times 10^{12}$ s^{-1} is determined, which is in good agreement with our estimate that is based purely on the steady-state experiments.

Electrostatic interactions between negatively charged **SWNT/pyrene**$^-$ and positively charged **MP**$^{8+}$ (i.e., M = Zn, H_2, Fe, and Co) were tested in a series of investigations. These include microscopy (i.e., transmission electron microscopy (TEM) and atomic force microscopy (AFM)) and spectroscopy (i.e., absorption and fluorescence spectroscopy). Figure 4 shows TEM photographs of **SWNT/pyrene**$^-$ samples, where we found linear objects tens of nanomenters in diameter, while their lengths reached several micrometers. Metal nanoparticles are absent due to the thermal and acid treatment of the nanotubes prior to the immobilization of the water-soluble **pyrene**$^-$ derivatives. In addition, the presence of small-diameter bundles proves that our **SWNT** approach toward water-soluble **SWNT/pyrene**$^-$ ensembles exfoliates individual SWNT from the original carbon nanotube bundles. Visualization of the negatively charged **SWNT/pyrene**$^-$ and positively charged **MP**$^{8+}$ ensembles through AFM reveals the presence of two to three isolated nanotubes interacting in the buffer solution, as is nicely demonstrated in Figure 5.

SWNT/Pyrene$^-$**/ZnP**$^{8+}$**.** In the next step, we employed absorption spectroscopy to test the interplay between **SWNT/pyrene**$^-$ and **ZnP**$^{8+}$. First, we titrated **ZnP**$^{8+}$ solutions with several concentrations of **SWNT/pyrene**$^-$. A representative example is given in Figure 6 for **SWNT/3**, from which we observe the following changes. First, we note red-shifts of the Soret- and Q-band features of **ZnP**$^{8+}$. The bands at 435, 565, and 605 nm shift to 439, 569, and 609 nm, respectively. Second,

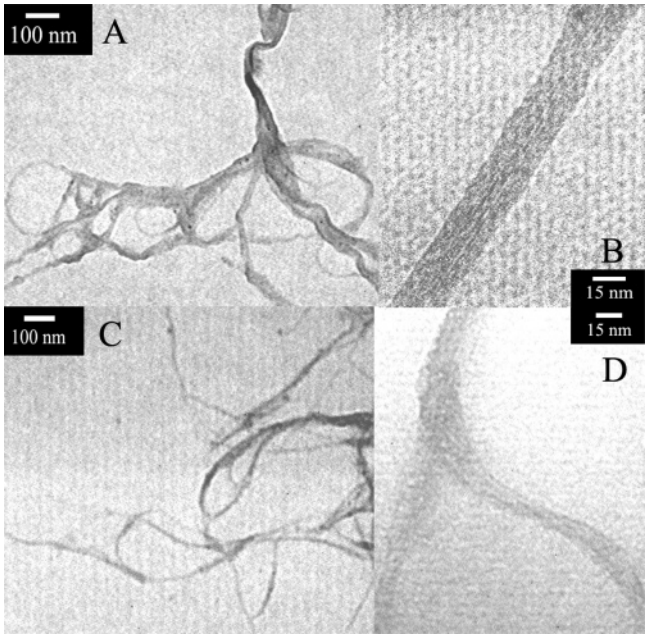

Figure 4. Transmission electron micrographs of purified pristine **SWNT** at low (a) and high (b) magnifications and water-soluble **SWNT/3** at low (c) and high (d) magnifications. The absence of metal nanoparticle impurities and the presence of thinner bundles in **SWNT/3** are evident due to the purification process followed and the solubilization/dispersion upon immobilization of water-soluble **pyrene**$^-$ onto **SWNT**, respectively.

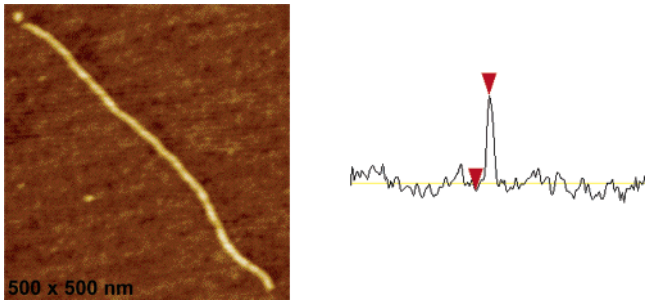

Figure 5. Atomic force microscopy images of **SWNT/pyrene**$^-$**/H$_2$P**$^{8+}$, showing the presence of isolated nanotubes. The height measure corresponds to 1.2 nm.

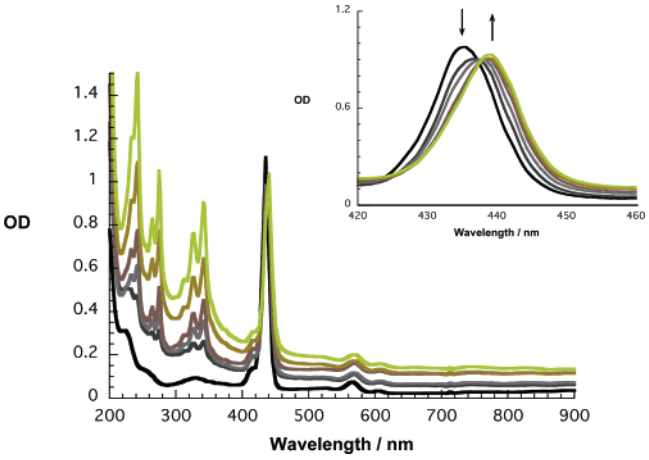

Figure 6. Absorption spectra of a dilute aqueous solution of **ZnP**$^{8+}$ upon addition of several concentrations of **SWNT/3**. The 420−460 nm range is amplified in the inset.

we see the presence of two isosbestic points at 426 and 437 nm. Finally, we find that the Soret transition at the endpoint of the titration has a slightly larger half-width and a slightly lower

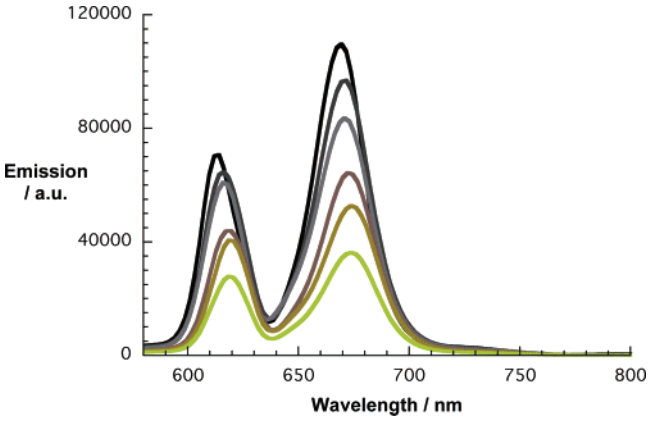

Figure 7. Fluorescence spectra of a dilute aqueous solution of **ZnP**$^{8+}$ upon addition of **SWNT/3** (complementary to Figure 6). Excitation wavelength is 437 nm.

extinction. All these data indicate a successful **SWNT/pyrene**$^-$/**ZnP**$^{8+}$ complex formation, driven by electrostatic interactions between **pyrene**$^-$ and **ZnP**$^{8+}$. The exact same changes were noted when **ZnP**$^{8+}$ was titrated with **1**, **2**, and **4**. Important is the fact that the typical van Hove singularities (i.e., 660, 745, 830, and 888 nm) of the **SWNT** remain unaffected by the **ZnP**$^{8+}$ association.

The absorption features of **ZnP**$^{8+}$ containing variable concentrations of just **pyrene**$^-$ — no SWNT, not shown — represent an important reference experiment. Essentially, the shifts are superimposable with those observed upon **SWNT/pyrene**$^-$ addition (i.e., 435 nm → 439 nm; 565 nm → 570 nm; 605 nm → 609 nm). The same isosbestic points developed at 426 and 437 nm. All these experiments lead to the conclusion that electrostatic forces are selective tools for associating **SWNT**s with **ZnP**. Long-range interactions, such as $\pi-\pi$ stacking, could not be confirmed for **SWNT** and **ZnP** solely on the basis of absorption spectroscopy.

Control tests were carried out by following the spectral changes for **SWNT/pyrene**$^-$ using a negatively charged **ZnP**$^{8-}$. Repulsive forces between the two negatively charged species are reflected by the lack of appreciable changes. Figure S3 (Supporting Information) summarizes a representative titration experiment.

Regarding the electron donor (i.e., **ZnP**)−acceptor (i.e., **SWNT**) interactions, fluorescence spectroscopy proved to be a very sensitive tool for their study. In the corresponding assays we recorded the **ZnP**$^{8+}$ fluorescence (i.e., $\lambda_{max} = 613$ and 668 nm; $\Phi = 0.04$; $\tau = 2.6$ ns) in the absence and in the presence of variable **SWNT/pyrene**$^-$ concentrations, generated by exciting at one of the isosbestic points — for example at 437 nm. As can be seen in Figure 7, when **SWNT/pyrene**$^-$ is present the **ZnP**$^{8+}$ fluorescence decreases with an exponential relationship relative to the **SWNT/pyrene**$^-$ concentration, until a plateau value is reached, where the complexation of **ZnP**$^{8+}$ is assumed to be complete and the effective concentration of **SWNT/pyrene**$^-$/**ZnP**$^{8+}$ is on the order of >90%. Please note that a purely diffusion driven process can be ruled out on the basis of the applied **SWNT/pyrene**$^-$ concentrations and the short lifetime of the **ZnP**$^{8+}$ singlet excited state (vide supra). Also, the fluorescence shifts progressively to the red (i.e., 613 nm → 619 nm; 668 nm → 674 nm). This trend parallels the changes seen in the absorption spectra. Finally, the monoexponential fluorescence decay, in the absence of **SWNT/pyrene**$^-$, is substituted, in the presence of **SWNT/pyrene**$^-$, by a decay function that is best represented by a biexponential rate law. We see a long-lived (i.e., 2.6 ± 0.1 ns) component and a short-lived (i.e., 0.22 ± 0.05 ns) component, which are related to the unquenched fluorescence in free **ZnP**$^{8+}$ and the quenched fluorescence in immobilized **ZnP**$^{8+}$ (i.e., **SWNT/pyrene**$^-$/**ZnP**$^{8+}$), respectively. Overall, the two lifetimes are maintained throughout the titration assay. Important is that with increasing **SWNT/pyrene**$^-$ concentration, the pre-exponential factor of the short-lived part increases, while that of the long-lived part falls steadily. Ultimately, the plateau region is reached, where only the short-lived component is monitored. Addition of acid restores the original **ZnP**$^{8+}$ fluorescence intensity, concomitant with the disappearance of the short-lived component and the reappearance of the long-lived component.

When **ZnP**$^{8+}$ is brought together with just **pyrene**$^-$, the picture deviates substantially from what has been concluded from the absorption spectra. As Figure S4 (Supporting Information) indicates, only red-shifts of the fluorescence peaks — although much weaker — occur. The 613 and 668 nm peaks shift to 617 and 671 nm, respectively. However, no quenching of the steady-state fluorescence or changes in the fluorescence lifetime is seen. A tentative hypothesis implies electrostatic **pyrene**$^-$/**ZnP**$^{8+}$ binding without meaningful photophysical consequences for photoexcited **ZnP**$^{8+}$.

In the last step, we tested the fluorescence behavior of **ZnP**$^{8-}$ in the absence and in the presence of **SWNT/pyrene**$^-$. At the beginning of the titration experiment, the characteristic **ZnP**$^{8-}$ fluorescence is seen, which manifests itself through a set of maxima at 612 and 665 nm. The fluorescence decay, as measured at both maxima, is monoexponential, from which a lifetime of 2.8 ± 0.1 ns is derived.[20] When variable amounts of **SWNT/pyrene**$^-$ were added, no overall changes were detected, except a 15% fluorescence quenching, which is attributed to competitive light absorption at the excitation wavelength.

On the basis of the aforementioned results we reach the following conclusion. The decrease of fluorescence intensity in **ZnP**$^{8+}$, the shift of the **ZnP**$^{8+}$ fluorescence, and evidence for a short-lived emissive component, which is invariant throughout the titration assay — all realized upon addition of **SWNT/pyrene**$^-$ — suggest a static quenching event inside a well-defined supramolecular **SWNT/pyrene**$^-$/**ZnP**$^{8+}$ complex. In **SWNT/pyrene**$^-$/**ZnP**$^{8+}$, the fluorescent state of **ZnP**$^{8+}$, which is a good electron donor, is quenched by electron transfer to the electron-accepting **SWNT** and, accordingly, substituted by a long-lived charge-separated state.

To shed light on the nature of the product evolving from this electron-transfer deactivation, complementary transient absorption measurements (i.e., 8 ns laser pulses at 532 nm) were necessary. Excitation at 532 nm, which guarantees irradiation into the Q-band absorption of **ZnP**$^{8+}$ while leaving **pyrene**$^-$ untouched, brings about the following triplet characteristics (i.e., Figure S5, Supporting Information): transient minimum and maximum at 540 and 835 nm, respectively. This triplet excited state decays in the absence of molecular oxygen to the singlet ground state with a time constant of $\sim 10^5$ s^{-1}.[26]

The picture associated with the nanosecond absorption

(26) Rodriguez, J.; Kirmaier, C.; Holten, D. *J. Am. Chem. Soc.* **1989**, *111*, 6500.

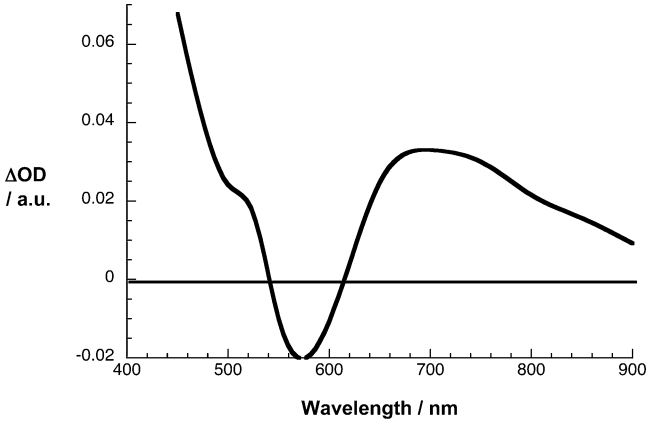

Figure 8. Differential absorption spectrum (visible and NIR) obtained upon nanosecond flash photolysis (532 nm) of **SWNT/3/ZnP^{8+}** in nitrogen-saturated solutions with a time delay of 100 ns.

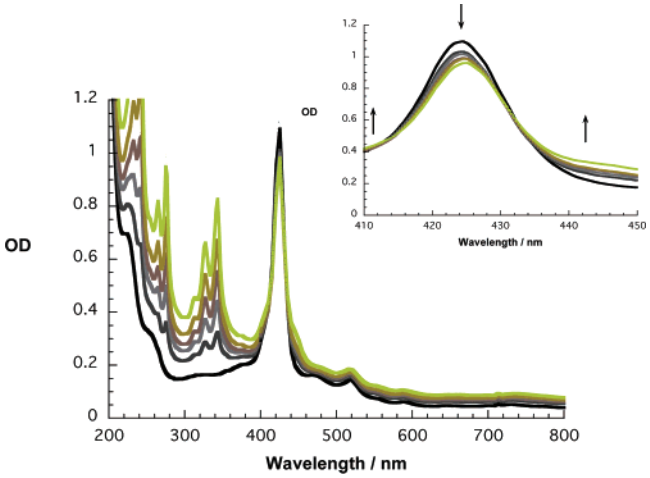

Figure 9. Absorption spectra of a dilute aqueous solution of **H$_2$P^{8+}** upon addition of several concentrations of **SWNT/1**. The 410−450 nm range is amplified in the inset.

spectroscopy in the presence of **SWNT/pyrene$^-$** (i.e., **3**) is notably different. Despite the unequivocal excitation of **ZnP^{8+}** at 532 nm, no porphyrin triplet−triplet absorption was found at short delay times following the 8 ns laser pulse in oxygen-free solutions. Instead, a new transient develops as a result of the rapid intrahybrid deactivation of the **ZnP^{8+}** excited state. A key feature of the new product is a broad transition between 600 and 900 nm (see Figure 8). This new transient resembles the one-electron-oxidized π-radical cation of **ZnP^{8+}**.[27] Due to the large spatial separation between the oxidized **ZnP^{8+}** and reduced **SWNT**, the radical ion pair features decay rather slowly, with a lifetime of 1.6 μs. The charge recombination process is governed by a monoexponential recovery of the singlet ground state rather than population of a porphyrin triplet excited state. Again, bringing just **pyrene$^-$** and **ZnP^{8+}** together leads exclusively to the formation of the above-described **ZnP^{8+}** triplet characteristics, due to the lack of electron donor−acceptor deactivation.

SWNT/Pyrene$^-$/H$_2$P^{8+}. As far as the absorption spectra are concerned, titration of **H$_2$P^{8+}** with **SWNT/pyrene$^-$** leads to minute alterations. The inset to Figure 9 corroborates that the Soret band is subject to only a moderate red-shift of 1 nm, which is complemented by clean isosbestic points at 413 and 432 nm. In contrast to the aforementioned **ZnP^{8+}** case, none of the Q-bands (i.e., 518, 548, 587, and 647 nm) seem to shift at all. Apparently, **H$_2$P^{8+}** is much less susceptible to electronic perturbations.

Our findings are still in agreement with an electrostatically driven association of **SWNT/pyrene$^-$/H$_2$P^{8+}**. Tests on the electrostatic attractions in **pyrene$^-$/H$_2$P^{8+}** and electrostatic repulsion between **SWNT/pyrene$^-$** and **H$_2$P^{8-}** further proved this hypothesis. For example, an experiment with **pyrene$^-$/H$_2$P^{8+}** gave rise to the same 1 nm red-shift, while no appreciable changes were seen when titrating **H$_2$P^{8-}** with **SWNT/pyrene$^-$**.

Interestingly, one of the **SWNT** transitions, namely, the one typically seen around 745 nm (i.e., E_{22} semiconductor transitions), is perturbed by additions of **H$_2$P^{8+}**. For **1**, **2**, and **3** the band shifts to 736, 738, and 734 nm, respectively. The remaining E_{22} semiconductor transitions at 660, 830, and 890 nm, on the other hand, were not affected. It is, however, unclear at present why this trend evolves exclusively for **H$_2$P^{8+}**, while **ZnP^{8+}** does not give any analogous shifts.

In steady-state experiments, the **H$_2$P^{8+}** fluorescence is characterized by maxima at 655 and 715 nm (see Figure S6, Supporting Information). Evidence for the electron-transfer deactivation came from titration experiments with variable **SWNT/pyrene$^-$** concentrations. Specifically, upon excitation at 432 nm, which corresponds to the isosbestic point of the ground-state absorption, a **SWNT/pyrene$^-$** concentration-dependent decrease in fluorescence intensity is seen. A closer inspection reveals, however, that the quenched **H$_2$P^{8+}** fluorescence (i.e., at 655 and 715 nm) is not accompanied by any appreciable red- or blue-shifts. This tracks the trend seen in the ground-state spectrum upon **SWNT/pyrene$^-$/H$_2$P^{8+}** association.

Prior to the addition of **SWNT/pyrene$^-$**, the fluorescent signal of **H$_2$P^{8+}** is well fitted by a monoexponential decay, for which a lifetime of 10.5 ± 0.5 ns was determined in deoxygenated aqueous solutions. Similar to the case with **SWNT/pyrene$^-$/ZnP^{8+}**, after addition of **SWNT/pyrene$^-$**, the fluorescent signal of **H$_2$P^{8+}** exhibits a double-exponential decay with lifetimes of 10.5 ± 0.5 and 0.32 ± 0.05 ns. An interpretation implies that the fast decaying component corresponds to intrahybrid electron-transfer quenching within **SWNT/pyrene$^-$/H$_2$P^{8+}**, while the slow decay represents deactivation in free **H$_2$P^{8+}**, not immobilized by **SWNT/pyrene$^-$**. The pre-exponential factors vary throughout the titration — the one associated with the 0.32 ± 0.05 ns lifetime increases with increasing **SWNT/pyrene$^-$**, while that of the 10.5 ± 0.5 ns lifetime decreases steadily.

In summary, steady-state and time-resolved fluorescence measurements testify that a rapid electron-transfer decay of the **H$_2$P^{8+}** singlet excited-state prevails in the **SWNT/pyrene$^-$/H$_2$P^{8+}** assemblies. Thus, to confirm the electron deactivation in **SWNT/pyrene$^-$/H$_2$P^{8+}**, transient absorption spectroscopy — following 8 ns laser excitation at 532 nm — was performed with **H$_2$P^{8+}** in the absence and in the presence of **SWNT/pyrene$^-$**.

In the absence of **SWNT/pyrene$^-$** (i.e., **3**), differential absorption spectra, recorded ca. 100 ns after the short laser pulse for a deoxygenated aqueous solution of **H$_2$P^{8+}**, are characterized by strong bleaching of the porphyrin Soret band and Q-band absorptions at 425 and 550 nm, respectively (not shown). Further in the red, an instantaneous formation of broad absorptions at wavelengths >600 nm, including a distinct maximum at 770

(27) Guldi, D. M.; Neta, P.; Hambright, P. *J. Chem. Soc., Faraday Trans.* **1992**, 88, 2013 and references therein.

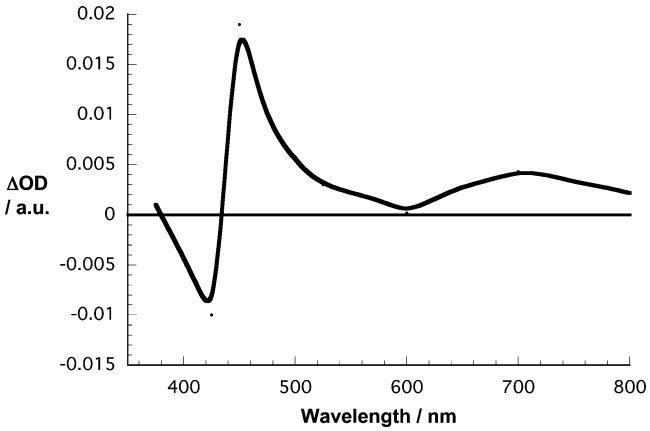

Figure 10. Differential absorption spectrum (visible and NIR) obtained upon nanosecond flash photolysis (532 nm) of **SWNT/3/H_2P^{8+}** in nitrogen-saturated solutions with a time delay of 100 ns.

nm, is discernible. These spectral features are attributes of the long-lived **H_2P^{8+}** triplet excited state.[26] In sharp contrast, the transient absorption changes for **SWNT/pyrene$^-$/H_2P^{8+}** reveal the characteristic broad band of one-electron-oxidized π-radical cation **H_2P^{8+}** that absorbs strongly in the visible region around 700 nm.[27] Figure 10 depicts these characteristics for **SWNT/3/H_2P^{8+}** with a time delay of 100 ns. In the case of **3**, the lifetime of the transient radical pair is 2.4 μs; this is significantly longer-lived relative to what was seen in the case of **SWNT/3/ZnP^{8+}** (vide supra). Considering that among the two porphyrins **ZnP^{8+}** is the better electron donor, our finding is the first indication that also in SWNT — similar to the electron-accepting C_{60}^{9-} — charge recombination dynamics are located in the Marcus-inverted region,[28] where kinetics slow down substantially with increasing free energy change (i.e., $-\Delta G$).

SWNT/Pyrene$^-$/CoP^{8+} and SWNT/Pyrene$^-$/FeP^{8+}. Spectral transformations associated with **CoP^{8+}** and **FeP^{8+}** were followed spectroscopically. A dilute aqueous solution of **CoP^{8+}** was titrated with **SWNT/pyrene$^-$**. Figure S7 (Supporting Information) shows that a clean conversion from **CoP^{8+}** to **SWNT/pyrene$^-$/CoP^{8+}** is observed, as evidenced by an isosbestic point at 446 nm and through red-shifts of the Soret and Q-bands. In the case of **1** and **3**, the maxima at 438, 552, and 591 nm shift to 440, 557, and 596 nm, respectively. Even stronger red-shifts were observed for **2** to 443, 560, and 600 nm. Interestingly, in **2** the carboxylic acid is directly linked to the pyrene core. Perhaps a closer proximity between the two π-systems contributes toward an enhanced electronic perturbation of the porphyrin macrocycle.

Relative to **SWNT/pyrene$^-$/CoP^{8+}**, the absorption changes accompanied with the formation of **SWNT/pyrene$^-$/FeP^{8+}** were different. In particular, prior to the addition of **SWNT/2** the following maxima were recorded: 422 nm (i.e., Soret band) and 625 and 661 nm (i.e., Q-band). While for **SWNT/pyrene$^-$/FeP^{8+}** the Soret band reveals the usual red-shift to 436 nm, the Q-band transitions shift surprisingly to the blue with new maxima at 598 and 637 nm (Figure S8, Supporting Information, illustrates these shifts). However, we cannot offer at this stage of the investigation any meaningful rationalization for the observed trend.

(28) Marcus, R. A. *Angew. Chem., Int. Ed. Engl.* **1993**, *32*, 1111.

Conclusions

We accomplished the integration of **SWNT**s, several water-soluble **pyrene$^-$**, and a series of water-soluble porphyrins into functional nanohybrids through a combination of associative van der Waals and electrostatic interactions. The **SWNT** functions as electron acceptor, while **MP^{8+}** metalloporphyrins are employed as excited-state electron donors. Crucial for the binding studies were **SWNT/pyrene$^-$** templates that bear carboxylate or sulfonate appendages. These negatively charged groups function (i) as promoters for suspending **SWNT** samples in aqueous media and (ii) as anchors for interaction with one or several pyridinium headgroups present in the different **MP^{8+}**.

Spectroscopic (i.e., absorption and fluorescence) and microscopic (i.e., AFM and TEM) methods were used to characterize the resulting **SWNT/pyrene$^-$** and **SWNT/pyrene$^-$/MP^{8+}**. Important for our steady-state and time-resolved work was that all the novel nanohybrids formed stable suspensions in aqueous media. A key feature of our **SWNT/pyrene$^-$** and **SWNT/pyrene$^-$/MP^{8+}** systems is that an efficient debundling was achieved, which in some cases gave isolated nanohybrid structures.

We could demonstrate with the help of transient absorption and fluorescence measurements that **SWNT** serve as the electron acceptor component in **SWNT/pyrene$^-$/MP^{8+}** (i.e., **H_2P^{8+}** and **ZnP^{8+}**). Intrahybrid electron transfer occurs on the 200−300 ps time scale and evolves from the photoexcited **H_2P^{8+}** and **ZnP^{8+}** to **SWNT**. This event leads to the reduction of the electron-accepting **SWNT** and oxidation of the electron-donating **MP^{8+}**. The radical ion pairs are long-lived and benefit from charge recombination dynamics that are located in the Marcus-inverted region.

Experimental Section

Preparation of SWNT/Pyrene$^-$. Water-soluble **SWNT**s were obtained in analogy to previous work, using 1-pyreneacetic acid (**1**), 1-pyrenecarboxylic acid (**2**), 1-pyrenebutyric acid (**3**), and 8-hydroxy-1,3,6-pyrenetrisulfonic acid (**4**) (**pyrene$^-$**).[18b] However, to reduce the amount of free pyrene in solution, **SWNT/pyrene$^-$** complex was allowed to precipitate, and the centrifuged solid was resolubilized in water.

Femtosecond transient absorption studies were performed with 387 nm laser pulses (1 kHz, 150 fs pulse width) from an amplified Ti:sapphire laser system (Clark-MXR, Inc.). Nanosecond laser flash photolysis experiments were performed with 532-nm laser pulses from a Quanta-Ray CDR Nd:YAG system (6 ns pulse width) in a front face excitation geometry. Fluorescence lifetimes were measured with a Laser Strobe fluorescence lifetime spectrometer (Photon Technology International) with 337 nm laser pulses from a nitrogen laser fiber-coupled to a lens-based T-formal sample compartment equipped with a stroboscopic detector. Details of the Laser Strobe systems are described on the manufacture's web site. Emission spectra were recorded with an SLM 8100 spectrofluorometer. The experiments were performed at room temperature. Each spectrum represents an average of at least five individual scans, and appropriate corrections were applied whenever necessary.

Synthesis. Chemicals and solvents were used as received unless otherwise noted. Solvents were dried using standard procedures. Column chromatography was performed on silica gel 32−63, 60 Å (MP Biomedicals). ^{1}H and ^{13}C NMR spectra were recorded on an Avance 300 instrument (Bruker Analytische Messtechnik GmbH). FAB mass spectrometry was performed with Micromass Zabspec and Varian MAT 311A machines. Standard UV/vis spectra were recorded on a Shimadzu

UV-3102 PC UV/vis NIR scanning spectrophotometer. IR spectra were taken with a Bruker Vector 22 spectrometer.

$CoBr_8$. 5,10,15,20-Tetrakis-(4'-*tert*-butyl-2',6'-bis(bromomethyl)-phenyl)porphyrin[29] (150 mg, 0.094 mmol), $CoBr_2$ (75 mg, 0.34 mmol), and sodium acetate (28 mg, 0.34 mmol) were dissolved in THF (25 mL). The reaction mixture was heated in the dark for 24 h (bath temperature 60 °C). The solvent was removed and the residue chromatographed on silica gel with CH_2Cl_2/hexanes 30:70) as eluent. Yield 76 mg (49%) of a dark orange solid; mp > 200 °C (dec). ^{1}H NMR (300 MHz, $CDCl_3$, 25 °C): δ 14.94 (br s, 8H, β-pyrr), 9.74 (br s, 8H, Ar−H), 5.80 (br s, 16H, CH_2), 2.65 (br s, 36H, *t*-Bu). ^{13}C NMR (75 MHz, $CDCl_3$, 25 °C): δ 154.60, 148.99, 144.50 (2C), 129.09 (2C), 35.39, 34.34, 31.43. MS (FAB, NBA): *m*/*z* 1639 (M^+), 1560 (M^+ − Br), 1478 (M^+ − 2Br). UV/vis (CH_2Cl_2): λ_{max} (ϵ, M^{-1} cm^{-1}) 415 (290 000), 531 (15 500), 564 (6800). IR (KBr): ν 2963, 2867, 1635, 1364, 1349, 1261, 1213, 1074, 1001, 884, 755, 717. Anal. Calcd for $C_{68}H_{68}Br_8CoN_4$ (1639.46): C, 49.82; H, 4.18; N, 3.42. Found: C, 49.92; H, 4.21; N, 3.42.

CoP^{8+}. $CoBr_8$ (75 mg, 0.046 mmol) was dissolved in 4-*tert*-butylpyridine (7.4 mL, 6.78 g, 50.2 mmol). The mixture was heated in the dark for 5 days (bath temperature 140 °C). The excess of 4-*tert*-butylpyridine was removed in vacuo, and the residue was suspended in diethyl ether, filtered, and thoroughly washed with diethyl ether. The solid was dissolved in a little CH_2Cl_2 and layered with diethyl ether. The precipitate was collected and washed with diethyl ether. The dissolving and precipitating procedure was repeated three times. The residue was dried in high vacuo. Yield 35 mg (65%) of an orange solid; mp > 220 °C (dec). ^{1}H NMR (300 MHz, $CDCl_3$, 25 °C): δ 9.51 (br s, 16H, α-pyridine), 9.35 (br s, 8H, β-pyrr), 7.83 (br s, 16H, β-pyridine), 6.31 (br s, 8H, Ar−H), 5.53 (m, 16H, CH_2), 1.29 (br.s, 72H, *t*-Bu-pyridine), 1.13 (br s, 36H, *t*-Bu). ^{13}C NMR (75 MHz, $CDCl_3$, 25 °C): δ 173.20, 155.49, 147.58, 143.65, 138.84, 135.12, 126.13, 121.46, 112.41, 62.88, 38.15, 36.46, 32.57, 31.44. UV/vis (CH_2Cl_2): λ_{max} (ϵ, M^{-1} cm^{-1}) 439 (205 000), 549 (15 000), 586 sh (2500). IR (KBr): ν 2964, 2924, 2865, 1638, 1562, 1461, 1372, 1274, 1163, 1113, 1061, 897, 723.

$FeBr_8$. 5,10,15,20-Tetrakis-(4'-*tert*-butyl-2',6'-bis(bromomethyl)-phenyl)porphyrin (100 mg, 0.063 mmol), iron(II) bromide (50 mg, 0.23 mmol), and sodium acetate (5 mg, 0.062 mmol) were dissolved in THF (20 mL). The reaction mixture was heated for 4 h under reflux. The solvent was removed and the residue chromatographed on silica gel with CH_2Cl_2 as eluent to remove unreacted starting material. The product was finally eluted with ethyl acetate. **$FeBr_8$** was crystallized from $CHCl_3$/hexanes to give dark blue microcrystals. Yield 78 mg (76%); mp > 200 °C (dec). ^{1}H NMR (300 MHz, $CDCl_3$, 25 °C): δ 82.1 (br s, pyrr. H), 16.8 (br s, *m*-Ar−H), 14.8 (br s, *m*-Ar−H), 9.0, 4.5, 2.8. MS (FAB, NBA): *m*/*z* 1636 (M^+), 1557 [($M - Br^+$). UV/vis (CH_2Cl_2): λ_{max} (ϵ, M^{-1} cm^{-1}) 365 sh (50 000), 392 (62 200) 422 (90 700), 508 (12 700), 576 (6300), 652 (4500). IR (KBr): ν 2955, 2861, 1527, 1478, 1201, 1102, 1069, 997, 802, 752. Anal. Calcd for $C_{68}H_{68}Br_8FeN_4$−OH·$CHCl_3$ (1762.74): C, 46.75; H, 3.98; N, 3.16. Found: C, 46.61; H, 3.78; N, 2.70.

FeP^{8+}. $FeBr_8$ (50 mg, 0.031 mmol) was dissolved in a mixture of 4-*tert*-butylpyridine (0.18 mL, 168 mg, 1.240 mmol) and toluene (20 mL). The mixture was refluxed for 12 h. The solvent was removed and the residue dissolved in dry methanol. Dry diethyl ether was added to precipitate the desired cationic porphyrin. The dissolving/precipitation procedure was repeated twice to give a dark greenish powder. Yield 60 mg (71%); mp > 200 °C (dec). ^{1}H NMR (300 MHz, D_2O, 25 °C): δ 63.9 (br s, β-pyrr), 10.4, 6.1, 2.6, 1.2. UV/vis (H_2O): λ_{max} (relative intensity) 334.5 (sh), 421.5 (1.00), 480.5 (0.14), 516.5 (0.09), 560 (0.05), 624.5 (0.04), 661 (0.05). IR (KBr): ν 3116, 3040, 2965, 2871, 1638, 1461, 1114, 1006, 852, 806.

Acknowledgment. This work was carried out with partial support from the EU (RTN network "WONDERFULL"), MIUR (PRIN 2004, prot. 2004035502), DFG (SFB 583), and the Office of Basic Energy Sciences of the U.S. Department of Energy. This is document NDRL-4606 from the Notre Dame Radiation Laboratory.

Supporting Information Available: NIR absorption spectra, fluorescence spectra, and nanosecond spectra of reference systems and those of **CoP^{8+}** and **FeP^{8+}**. This material is available free of charge via the Internet at http://pubs.acs.org.

JA050930O

(29) Jux, N. *Org. Lett.* **2000**, *2*, 2129.